DALTON

Paramagnetic tetrahedral dinitrosyliron complexes containing redox-active cyanomanganese ligands *

Francis L. Atkinson,[a] Nathan C. Brown,[a] Neil G. Connelly,[a] A. Guy Orpen,[a] Anne L. Rieger,[b] Philip H. Rieger[b] and Georgina M. Rosair[a]

[a] *School of Chemistry, University of Bristol, Bristol BS8 1TS, UK*
[b] *Department of Chemistry, Brown University, Providence, RI 02912, USA*

The redox-active cyanomanganese ligands *trans*-[Mn(CN)(CO)$_2${P(OEt)$_3$}(dppm)] (dppm = $Ph_2PCH_2PPh_2$), *cis*-[Mn(CN)(CO)$_2$(PEt$_3$)(dppe)] (dppe = $Ph_2PCH_2CH_2PPh_2$) and *trans*-[Mn(CN)(CO)(dppm)$_2$] reacted with [{Fe(μ-I)(NO)$_2$}$_2$] in CH_2Cl_2 to give the heterobinuclear complexes [FeI{(μ-NC)MnL$_x$}(NO)$_2$] {L$_x$ = *trans*-(CO)$_2$[P(OEt)$_3$](dppm) **1**, *cis*-(CO)$_2$(PEt$_3$)(dppe) **2** and *trans*-(CO)(dppm)$_2$ **3**}; the molecular structure of **3** is consistent with a tetrahedral iron(−I) centre bound to octahedral manganese(I) by a near linear Mn–CN–Fe bridge. The ESR spectra of complexes **1–3** are very similar to those of the tetrahedral Fe^{-I} complex $[FeI_2(NO)_2]^-$. Complexes **1–3** reacted with PPh_3 in the presence of $TlPF_6$ to give [Fe(PPh$_3$)-{(μ-NC)MnL$_x$}(NO)$_2$][PF$_6$] {L$_x$ = *trans*-(CO)$_2$[P(OEt)$_3$](dppm) $\mathbf{5}^+$, *cis*-(CO)$_2$(PEt$_3$)(dppe) $\mathbf{6}^+$ and *trans*-(CO)(dppm)$_2$ $\mathbf{7}^+$} which were also prepared from [Fe(PPh$_3$)$_2$(NO)$_2$][PF$_6$] and the appropriate cyanomanganese ligand in a 1 : 1 ratio; the related cation [Fe(PPh$_3$){(μ-NC)MnL$_x$}(NO)$_2$]$^+$ {L$_x$ = *trans*-(CO)$_2$[P(OPh)$_3$](dppm) $\mathbf{8}^+$} was generated in solution. The ESR spectra of complexes $\mathbf{6}^+$–$\mathbf{8}^+$ showed hyperfine coupling to N(O), P, N(C) and Mn, suggesting a structure similar to that of [Fe(PPh$_3$)(OPPh$_3$)(NO)$_2$]$^+$ with some delocalisation through the cyanide bridge to manganese. Treatment of 2 equivalents of *trans*-[Mn(CN)(CO)$_2${P(OEt)$_3$}(dppm)] or *cis*-[Mn(CN)(CO)$_2$(PEt$_3$)(dppe)] with [Fe(PPh$_3$)$_2$(NO)$_2$][PF$_6$] gave the heterotrinuclear complexes [Fe{(μ-NC)MnL$_x$}$_2$(NO)$_2$][PF$_6$] {L$_x$ = *trans*-(CO)$_2$[P(OEt)$_3$](dppm) $\mathbf{9}^+$ and *cis*-(CO)$_2$(PEt$_3$)(dppe) $\mathbf{10}^+$} which may also be prepared from the reaction of **1** with *trans*-[Mn(CN)(CO)$_2${P(OEt)$_3$}(dppm)] or **2** with *cis*-[Mn(CN)(CO)$_2$(PEt$_3$)(dppe)] in the presence of $TlPF_6$. Complexes **1**–$\mathbf{10}^+$, which contain diamagnetic Mn^I and paramagnetic Fe^{-I} centres, undergo oxidation and reduction at a platinum electrode in CH_2Cl_2. The Mn^{II} derivatives $\mathbf{3}^+$ and $\mathbf{7}^{2+}$ and the Fe^{-II} complex **7** have been generated in solution by ferrocenium ion oxidation or cobaltocene reduction respectively.

There is considerable current interest in the cyanide ion as either a terminal[1] or bridging[2–4] ligand, the latter particularly because of its ability to mediate intramolecular electron and/or energy transfer between two or more metal centres.[5] Our studies of octahedral carbonylcyanomanganese(I) complexes [Mn(CN)(CO)L$_x$] as redox-active ligands suggest that the extent to which intramolecular electron transfer can occur to a second metal site, through a cyanide bridge, may depend on the arrangement of the ancillary ligands (L$_x$) about manganese.[6] In addition, we have investigated the effects of varying the nature and geometry of the second metal site on intramolecular electron transfer, preparing bi- and tri-metallic complexes in which the cyanomanganese ligands are bound (*i*) to a second octahedral manganese site,[7,8] as in [Mn(CO)$_2$-L(L–L){(μ-NC)MnL$_x$}] [L = phosphine or phosphite, L–L = $Ph_2PCH_2PPh_2$(dppm) or $Ph_2PCH_2CH_2PPh_2$(dppe)], (*ii*) in [Ru(CO)$_2$(PPh$_3$)(*o*-$O_2C_6Cl_4$){(μ-NC)MnL$_x$}], which undergoes catecholate-based oxidation,[9] (*iii*) to square planar rhodium(I), *e.g.* in [RhCl(CO)$_2${(μ-NC)MnL$_x$}][10] and (*iv*) in linear complexes of copper(I), silver(I) and gold(I), *i.e.* [M′{(μ-NC)MnL$_x$}$_2$]$^+$ (M′ = Cu, Ag or Au).[11] In this paper we describe the synthesis of the bi- and tri-metallic complexes [FeI{(μ-NC)MnL$_x$}(NO)$_2$], [Fe(PPh$_3$){(μ-NC)MnL$_x$}(NO)$_2$]-[PF$_6$] and [Fe{(μ-NC)MnL$_x$}$_2$(NO)$_2$][PF$_6$] in which cyanomanganese ligands are bound to tetrahedral, paramagnetic [formally iron(−I)] dinitrosyliron centres. The effects of varying the ligands at Fe on the bonding in the Mn(μ-CN)-Fe skeleton, and of those at Mn on the stability of the (formal) Fe^{-I}–Fe^{-II} redox couple, have been studied by IR spectroscopy, particularly in the cyanide stretching region,[3,12] ESR spectroscopy, electrochemistry and crystal structure analysis of [FeI{(μ-NC)Mn(CO)(dppm)$_2$}(NO)$_2$] as its dichloromethane solvate.

* *Non-SI unit employed:* G = 10^{-4} T.

Results and Discussion

Complexes [FeIL(NO)$_2$] (L = cyanomanganese ligand)

The addition of 2 equivalents of *trans*-[Mn(CN)(CO)$_2$-{P(OEt)$_3$}(dppm)], *cis*-[Mn(CN)(CO)$_2$(PEt$_3$)(dppe)] or *trans*-[Mn(CN)(CO)(dppm)$_2$] to 1 equivalent of the dimer [{Fe(μ-I)(NO)$_2$}$_2$] in CH_2Cl_2 immediately gave dark brown solutions from which [FeI{(μ-NC)MnL$_x$}(NO)$_2$] {L$_x$ = *trans*-(CO)$_2$[P(OEt)$_3$](dppm) **1**, *cis*-(CO)$_2$(PEt$_3$)(dppe) **2** or *trans*-(CO)(dppm)$_2$ **3**} were readily isolated in *ca.* 60–70% yield as brown microcrystals. In addition, [FeI{(μ-NC)MnL$_x$}(NO)$_2$] **4** {L$_x$ = *trans*-(CO)$_2$[P(OPh)$_3$](dppm)} was generated *in situ* from [{Fe(μ-I)(NO)$_2$}$_2$] and *trans*-[Mn(CN)(CO)$_2${P(OPh)$_3$}-(dppm)] for spectroscopic studies.

Complexes **1–3** were characterised by elemental analysis, and by IR (Table 1) and ESR spectroscopy (see below). Each complex, and complex **4**, shows two nitrosyl bands and either one or two carbonyl bands (depending on the number of carbonyl ligands and their relative geometry) in the IR spectrum. The carbonyl bands are shifted to higher energies by 10–20 cm^{-1} when the manganese ligands (Table 2) are co-ordinated to the FeI(NO)$_2$ fragment, indicating that the electron density at the manganese centre is decreased. However, the carbonyl bands for the binuclear complexes are much closer in energy to those of the neutral Mn^I ligands than those of the corresponding Mn^{II} species, showing that complexes **1–4** retain the oxidation state Mn^I.

The energies of ν(NO) for complexes **1–4** (Table 1) are very similar but somewhat lower than those of $[FeI(PPh_3)(NO)_2]$ [ν(NO) 1792, 1739 cm^{-1}], implying that the cyanomanganese ligands are better net electron donors than PPh_3. However, the values of ν(NO) remain typical of 17-electron dinitrosyliron complexes rather than of 18-electron species,[14] showing that iron retains the formal oxidation state Fe^{-I}.

The co-ordination of a manganese ligand to the $FeI(NO)_2$ fragment causes only a small increase (0–10 cm^{-1}) in ν(CN). Several factors influence the energy of ν(CN) for a bridging cyanide ligand. The mechanical restraint imposed when a metal is N bound, forming a bridge, invariably causes an increase in the energy of ν(CN).[12] However, the observation of a net increase or decrease in ν(CN) will depend on electronic factors, mainly the extent to which the population of the C–N π* orbitals is affected by the σ- or π-electron donor or acceptor abilities of the C- and N-bound metal sites.[3,15] Increases in the energy of ν(CN) have usually been observed on co-ordination of the manganese ligands described herein, for example to $Ru(CO)_2(PPh_3)(o\text{-}O_2C_6Cl_4)$.[9] The small increase observed for $[FeI\{(\mu\text{-}NC)MnL_x\}(NO)_2]$ suggests $FeI(NO)_2$ to be a good π-accepting group.

On the basis of the similarities between the IR nitrosyl spectra of complexes **1–4** and those of other four-co-ordinate dinitrosyliron complexes,[15] the former are assumed to adopt a tetrahedral, or nearly so, structure. However, we have shown recently[16] that relatively small changes in the donor/acceptor properties of L and L′ can bring about significant structural distortions in $[FeLL'(NO)_2]^z$ fragments. In order, therefore, to make detailed comparisons with our earlier studies of complexes such as $[Fe(PPh_3)_2(NO)_2]^+$ and $[Fe(OPPh_3)(PPh_3)(NO)_2]^+$[16] we have determined the crystal structure of complex **3** as its dichloromethane solvate.

Crystals suitable for an X-ray diffraction study were grown by allowing a concentrated CH_2Cl_2 solution of **3** to diffuse into *n*-hexane at −10 °C. The molecular structure (Fig. 1) consists of an octahedral manganese centre co-ordinated to tetrahedral iron *via* the nitrogen atom of a bridging cyanide ligand. Selected bond lengths and angles are given in Table 3.

The mean Mn–P distances in *trans*-$[Mn(CN)(CO)(dppm)_2]^z$ [2.270(1)°, $z = 0$ and 2.346(5) Å, $z = 1$][6] can be used to indicate the oxidation state of manganese when such complexes act as ligands towards a second metal centre. The mean Mn–P distance in **3** (2.288 Å) is closer (although somewhat longer) to that in *trans*-$[Mn(CN)(CO)(dppm)_2]$, than that in *trans*-$[Mn(CN)(CO)(dppm)_2]^+$. The geometry about manganese is therefore consistent with the presence of Mn^{I}, and therefore Fe^{-I} (rather than Mn^{II} and Fe^{-II}), as also suggested by the IR (see above) and ESR (see below) spectra.

As in *trans*-$[Mn(CN)(CO)(dppm)_2]^z$ ($z = 0$ and 1), the largest distortions from regular octahedral geometry originate

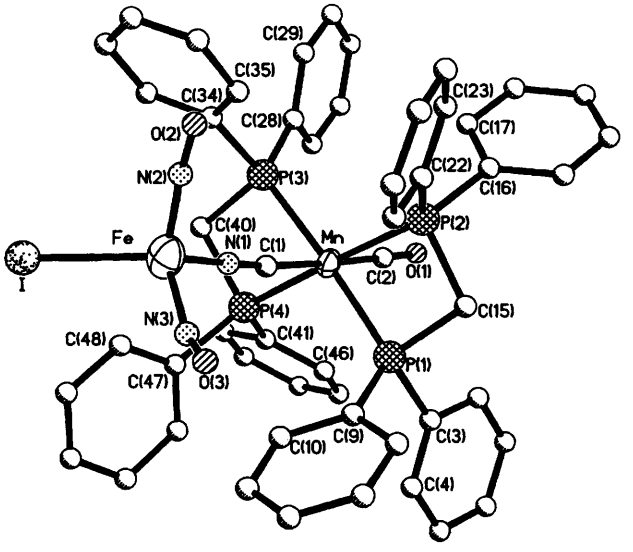

Fig. 1 Molecular structure of $[FeI\{(\mu\text{-}NC)Mn(CO)(dppm)_2\}(NO)_2]$ **3**. All hydrogen atoms have been omitted for clarity

Table 1 Analytical and IR spectroscopic data for $[FeL'_n\{(\mu\text{-}NC)MnL_x\}_{2-n}(NO)_2]^z$

	L_x	*n*	L′	*z*[c]	Colour	Yield (%)	Analysis (%)[a] C	H	N	IR[b]/cm^{-1} ν(CN)[d]	ν(CO)[e]	ν(NO)[f]
1	*trans*-$(CO)_2[P(OEt)_3](dppm)$	1	I^-	0	Brown	45	43.9 (43.9)	4.2 (4.0)	4.5 (4.5)	2082	(2008), 1928vs	1791, 1726
2	*cis*-$(CO)_2(PEt_3)(dppe)$	1	I^-	0	Brown	70	47.1 (46.9)	4.4 (4.4)	4.5 (4.7)	2100mw	1945, 1891ms	1794, 1729
3	*trans*-$(CO)(dppm)_2$	1	I^-	0	Brown	56	55.8 (55.7)	4.0 (4.0)	3.7 (3.8)	2080	1877	1789, 1724
4	*trans*-$(CO)_2[P(OPh)_3](dppm)$	1	I^-	0	Brown	*g*				2092	(2020), 1942vs	1792, 1726
5$^+$	*trans*-$(CO)_2[P(OEt)_3](dppm)$	1	PPh_3	1	Blue	78	51.3 (51.6)	4.6 (4.3)	3.2 (3.5)	2054	(2004), 1932vs	1800, 1746m
6$^+$	*cis*-$(CO)_2(PEt_3)(dppe)$	1	PPh_3	1	Blue	68	54.2 (54.1)	4.9 (4.6)	3.3 (3.6)	2071mw	1949, 1900ms	1805, 1749
7$^+$	*trans*-$(CO)(dppm)_2$	1	PPh_3	1	Blue	53	59.7 (60.0)	4.3 (4.2)	2.7 (3.0)	2042	1887	1797, 1744
8$^+$	*trans*-$(CO)_2[P(OPh)_3](dppm)$	1	PPh_3	1	Blue	*g*				2064	(2014), 1944vs	1802, 1747m
9$^+$	*trans*-$(CO)_2[P(OEt)_3](dppm)$	0	—	1	Brown	73	50.0 (49.9)	4.8 (4.6)	3.2 (3.4)	2067	(2005), 1930vs	1801, 1731m
10$^+$	*cis*-$(CO)_2(PEt_3)(dppe)$	0	—	1	Brown	50	53.8 (53.6)	5.1 (5.0)	3.5 (3.6)	2087	1949vs, 1895vs	1806, 1734m

[a] Calculated values in parentheses. [b] In CH_2Cl_2; strong absorptions unless otherwise stated, m = medium, w = weak, vs = very strong. [c] Cationic complexes analysed as $[PF_6]^-$ salts. [d] Medium unless otherwise stated. [e] Very weak A mode, forbidden under D_{4h} symmetry, in parentheses. [f] Higher energy absorption medium, lower energy absorption medium strong unless otherwise stated. [g] Complex not isolated, see text.

Table 2 Infrared spectra (in CH_2Cl_2) and formal oxidation potentials for cyanomanganese ligands[a]

Ligand	$E^{o'}$[b]/V	IR/cm^{-1} ν(CN)[c]	ν(CO)[d]
trans-$[Mn(CN)(CO)_2\{P(OEt)_3\}(dppm)]$	0.50	2079	(2001) 1914
trans-$[Mn(CN)(CO)_2\{P(OPh)_3\}(dppm)]$	0.64	2085	(2012) 1930
cis-$[Mn(CN)(CO)_2(PEt_3)(dppe)]$	0.77 (I) (0.32[e])	2090	1936, 1873
trans-$[Mn(CN)(CO)(dppm)_2]$	0.07	2080	1861
trans-$[Mn(CN)(CO)_2\{P(OEt)_3\}(dppm)]^+$	0.48		(2065) 1993
trans-$[Mn(CN)(CO)(dppm)_2]^+$	0.07	2104	1938

[a] Data taken from refs. 6 and 13 and refs. therein. [b] Reversible oxidation wave unless stated otherwise; I = irreversible. [c] Weak absorption. [d] Strong absorptions; very weak A mode in parentheses. [e] Reduction peak potential of *trans* product wave.

Table 3 Selected bond lengths (Å) and angles (°) for complex **3**·CH_2Cl_2

Mn–P(1)	2.283(3)	Mn–P(2)	2.293(4)	Mn–P(3)	2.289(3)
Mn–P(4)	2.286(4)	Mn–C(1)	1.953(14)	Mn–C(2)	1.795(13)
Fe–I	2.573(2)	Fe–N(1)	1.956(12)	Fe–N(2)	1.660(14)
Fe–N(3)	1.763(15)	P(1)–C(3)	1.837(12)	P(1)–C(9)	1.814(12)
P(1)–C(15)	1.846(12)	P(2)–C(15)	1.854(11)	P(2)–C(16)	1.826(11)
P(2)–C(22)	1.819(15)	P(3)–C(28)	1.828(11)	P(3)–C(34)	1.819(13)
P(3)–C(40)	1.837(12)	P(4)–C(40)	1.863(10)	P(4)–C(41)	1.822(15)
P(4)–C(47)	1.834(10)	O(1)–C(2)	1.169(16)	O(2)–N(2)	1.160(21)
O(3)–N(3)	0.995(21)	N(1)–C(1)	1.155(18)		

P(1)–Mn–P(2)	73.7(1)	P(1)–Mn–P(3)	175.2(1)
P(2)–Mn–P(3)	107.9(1)	P(1)–Mn–P(4)	104.7(1)
P(2)–Mn–P(4)	177.3(1)	P(3)–Mn–P(4)	73.9(1)
P(1)–Mn–C(1)	88.6(3)	P(2)–Mn–C(1)	91.3(4)
P(3)–Mn–C(1)	86.8(3)	P(4)–Mn–C(1)	90.8(4)
P(1)–Mn–C(2)	92.6(3)	P(2)–Mn–C(2)	87.4(4)
P(3)–Mn–C(2)	92.0(3)	P(4)–Mn–C(2)	90.5(4)
C(1)–Mn–C(2)	178.0(6)	I–Fe–N(1)	108.4(3)
I–Fe–N(2)	106.8(3)	N(1)–Fe–N(2)	111.8(5)
I–Fe–N(3)	111.4(5)	N(1)–Fe–N(3)	110.9(6)
N(2)–Fe–N(3)	107.6(8)	Fe–N(1)–C(1)	176.0(10)
Fe–N(2)–O(2)	165.0(13)	Fe–N(3)–O(3)	157.0(21)
Mn–C(1)–N(1)	175.4(11)	Mn–C(2)–O(1)	178.9(11)

from the chelating dppm ligand [P(1)–Mn–P(2) 73.7(1) and P(3)–Mn–P(4) 73.9(1)°]. Unlike in *trans*-[Mn(CN)(CO)(dppm)$_2$], the OC–Mn–CN axis in **3** is not tilted significantly (by only 0.7° here) with respect to the normal of the MnP_4 plane. The Mn–CO [1.795(13) Å] and Mn–CN [1.953(14) Å] bond lengths are close to typical values[17] for Mn–CO (1.808 Å) and Mn–CNR bonds (1.927 Å). The Mn(μ-CN)Fe skeleton is nearly linear [Mn–C(1)–N(1) 175.4(11), Fe–N(1)–C(1) 176.0(10)°].

The co-ordination geometry about iron is close to tetrahedral, the bond angles ranging from 107.6(8) to 111.8(5)°. The structure of **3** is therefore closer to those of complexes such as $[Fe(PPh_3)_2(NO)_2]^+$ [16] and $[FeI_2(NO)_2]^-$,[18] than that of the more distorted cation $[Fe(OPPh_3)(PPh_3)(NO)_2]^+$,[16] consistent with the similar ESR spectra of **3** and $[FeI_2(NO)_2]^-$ (see below). In agreement with the theory of Summerville and Hoffmann,[19] however, the angle (O)N–Fe–N(O) [111.8(5)°] (between two strong π-accepting ligands) is a little larger than the angle (C)N–Fe–I [108.4(3)°] (between two stronger π-donors, or weaker π-acceptors). The (O)N–Fe–N(O) angle is one of the smallest yet observed for a pseudotetrahedral dinitrosyl fragment.[16] Moreover, the nitrosyl ligands are strongly inwardly bent (the angle O···Fe···O is 93.2°) but with the $Fe(NO)_2$ group again essentially planar (the oxygens lie *ca.* 0.020 Å from the FeN_2 plane). The data for **3** fit the linear correlation between the angles (O)N–M–N(O) and O···M···O observed[16] for 54 other four-co-ordinate metal dinitrosyl complexes.

The cyclic voltammogram of complex **3**, in CH_2Cl_2 at a platinum disc electrode, shows a single, reversible oxidation wave at 0.28 V. By contrast, the cyclic voltammograms of **1** and **2** are very poorly defined; multiple scans show several ill-defined product peaks for both complexes suggesting that oxidation is followed by decomposition of the heterobinuclear units. A comparison of the oxidation potential of **3** with that of the free ligand *trans*-[Mn(CN)(CO)(dppm)$_2$] (Table 2) shows that the manganese centre is more difficult to oxidise when co-ordinated to the $FeI(NO)_2$ fragment ($\Delta E^{\circ\prime} = 0.21$ V). Similar increases in oxidation potential have been observed on co-ordination of *trans*-[Mn(CN)(CO)(dppm)$_2$] to *cis*-$RhCl(CO)_2$ ($\Delta E^{\circ\prime} = 0.14$ V)[10] and *cis*-$Ru(CO)_2(PPh_3)(o\text{-}O_2C_6Cl_4)$ ($\Delta E^{\circ\prime} = 0.09$ V),[9] again in accord with decreased electron density at manganese when the cyanide is N-bonded to iron. That $E^{\circ\prime}$ is shifted by a larger amount suggests $FeI(NO)_2$ to be a stronger acceptor than the Rh or Ru units, a suggestion also borne out by IR spectroscopy where **3** has the highest value of ν(CO) (1877 cm^{-1}, *cf.* 1874 and 1871 for the Rh and Ru complexes, respectively) and the smallest shift (from the free ligand) in ν(CN) (see above).

The reversibility of the oxidation wave of **3**, and its relatively low potential, suggested that $\mathbf{3}^+$ might be isolable using a mild one-electron oxidant. Complex **3** is indeed oxidised by the ferrocenium ion, but $\mathbf{3}^+$ is generated more conveniently by the direct reaction of *trans*-$[Mn(CN)(CO)(dppm)_2]^+$ with $[\{Fe(\mu\text{-}I)(NO)_2\}_2]$ in CH_2Cl_2. No product stable enough to be fully characterised could be isolated from the dark brown reaction mixture but the IR spectrum was consistent with the formation of the Mn^{II} complex $\mathbf{3}^+$ [ν(CN) 2120mw; ν(CO) 1952s; ν(NO) 1801m, 1735ms cm^{-1}]. The cyanide stretching frequency increases in energy by 40 cm^{-1} (*cf.* **3**), as found previously when the C-bound end of the Mn–CN–M′ unit in [M′(μ-NC)Mn(CO)(dppm)$_2$] [M′ = $Ru(CO)_2(PPh_3)(o\text{-}O_2C_6Cl_4)$[9] or $RhCl(CO)_2$[10]] was oxidised. The nitrosyl bands also shift to higher energy, by *ca.* 12 cm^{-1}, possibly as a consequence of the increased positive charge on the complex as a whole rather than electron transfer from iron to manganese through the cyanide bridge.

Complex **3** also shows a broad, irreversible peak at *ca.* −0.8 V which most likely corresponds to reduction at the iron centre. In the series $[FeLL'(NO)_2]^+$ (L, L′ = PPh_3 or $OPPh_3$), the reversibility of the reduction process decreases as L and L′ become better σ donors (worse π acceptors). The cation $[Fe(PPh_3)_2(NO)_2]^+$ is reduced ($E^{\circ\prime} = 0.37$ V) to $[Fe(PPh_3)_2(NO)_2]$ which is isolable (stabilised by the presence of two π-acceptor PPh_3 ligands); the reduction of $[Fe(OPPh_3)_2(NO)_2]^+$ (containing two σ-donating $OPPh_3$ ligands) is completely irreversible and at a much more negative potential [$(E_p)_{red} = -0.59$ V].[15] The irreversibility, and rather negative potential, of the reduction of **3** therefore implies that *trans*-[Mn(CN)(CO)(dppm)$_2$] functions as a net electron donor towards $FeI(NO)_2$ (as also suggested by IR spectroscopy).

Complexes $[Fe(PPh_3)L(NO)_2]^+$ (L = cyanomanganese ligand)

As noted above, the reduction of complex **3** results in decomposition even on the cyclic voltammetric time-scale. Given that the replacement of the σ donor $OPPh_3$ by PPh_3 in $[Fe(OPPh_3)(PPh_3)(NO)_2]^+$ stabilises[16] the neutral complex $[Fe(PPh_3)_2(NO)_2]$, it was anticipated that substitution of the σ donor, I^-, in complexes **1**–**3** by PPh_3 might similarly provide

more stable reduced species. Accordingly, the synthesis of complexes of the type $[Fe(PPh_3)\{(\mu\text{-}NC)MnL_x\}(NO)_2][PF_6]$ was investigated.

The complexes $[Fe(PPh_3)\{(\mu\text{-}NC)MnL_x\}(NO)_2][PF_6]$ can be prepared by reacting **1–3** respectively with PPh_3 in the presence of $TlPF_6$. However, a more convenient route exploits the substitutional lability of $[Fe(PPh_3)_2(NO)_2]^+$.[16] Thus, the addition of 1 equivalent of *trans*-$[Mn(CN)(CO)_2\{P(OEt)_3\}(dppm)]$, *cis*-$[Mn(CN)(CO)_2(PEt_3)(dppe)]$ or *trans*-$[Mn(CN)(CO)(dppm)_2]$ to $[Fe(PPh_3)_2(NO)_2][PF_6]$ in CH_2Cl_2 gave deep blue solutions from which $[Fe(PPh_3)\{(\mu\text{-}NC)MnL_x\}(NO)_2][PF_6]$ {L_x = *trans*-$(CO)_2[P(OEt)_3](dppm)$ $\mathbf{5}^+$, *cis*-$(CO)_2(PEt_3)(dppe)$ $\mathbf{6}^+$ or *trans*-$(CO)(dppm)_2$ $\mathbf{7}^+$} were isolated by precipitation with *n*-hexane and purification from CH_2Cl_2–*n*-hexane. The blue microcrystalline solids were characterised by elemental analysis, and by IR (Table 1) and ESR spectroscopy (see below). In addition, $[Fe(PPh_3)\{(\mu\text{-}NC)MnL_x\}(NO)_2][PF_6]$ $\mathbf{8}^+$ {L_x = *trans*-$(CO)_2[P(OPh)_3](dppm)$} was generated *in situ* from $[Fe(PPh_3)_2(NO)_2][PF_6]$ and *trans*-$[Mn(CN)(CO)_2\{P(OPh)_3\}(dppm)]$ for spectroscopic study.

The nitrosyl stretching frequencies of $\mathbf{5}^+$–$\mathbf{8}^+$ are higher in energy than those of **1–4** (for a given manganese ligand the two bands for complexes of the former set are *ca.* 10 and 20 cm^{-1} higher than for the latter), reflecting the increased positive charge on iron; a comparison with the nitrosyl bands of $[Fe(PPh_3)_2(NO)_2]^+$ and $[Fe(OPPh_3)(PPh_3)(NO)_2]^+$ [16] again shows that the cyanomanganese ligands are better net electron donors than PPh_3 and are comparable with $OPPh_3$. There is also a greater increase (13–26 cm^{-1}) in ν(CO) when the cyanomanganese(I) ligands are co-ordinated to $[Fe(PPh_3)(NO)_2]^+$ rather than to $FeI(NO)_2$ (Table 1). The stronger electron-withdrawing effect of $[Fe(PPh_3)(NO)_2]^+$ causes a substantial decrease (*ca.* 30–40 cm^{-1}) in the energy of the cyanide IR stretching frequency (Table 1) when compared with the data for complexes of $FeI(NO)_2$. The increased population of the π* CN orbitals, brought about by enhanced π back donation from Mn to the cyanide bridge, outweighs the mechanical effect on ν(CN).

The cyclic voltammogram of $\mathbf{7}^+$ is similar to that of **3** in showing a reversible oxidation wave at 0.42 V. The more positive shift in potential from the value for the free ligand ($\Delta E^{o\prime} = 0.35$ V) again suggests that the cationic $Fe(PPh_3)(NO)_2^+$ unit withdraws more electron density from manganese than the neutral $FeI(NO)_2$ unit [also shown by the increase in ν(CO) to 1887 cm^{-1} for $\mathbf{7}^+$]. The cyclic voltammograms of $\mathbf{5}^+$ and $\mathbf{6}^+$ are somewhat better defined than those of **1** and **2** but still relatively uninformative. Complex $\mathbf{5}^+$ shows a broadened oxidation peak [$(E_p)_{ox} = 1.04$ V] with reduction peaks at 0.72 V and 0.32 V. The latter, which has a relatively low current, may be due to the reduction of $[Fe(PPh_3)_2(NO)_2]^+$ [16] formed during the decomposition of $\mathbf{5}^{2+}$. The cyclic voltammogram of $\mathbf{6}^+$ shows an irreversible oxidation peak at 1.21 V, with a product reduction peak at 0.79 V, behaviour indicative of the expected oxidative isomerisation at the *cis*-manganese centre.[13]

The reversibility and potential of the oxidation wave for $\mathbf{7}^+$ suggested that $\mathbf{7}^{2+}$ might be isolable. Direct oxidation of $\mathbf{7}^+$ with $[Fe(\eta\text{-}C_5H_5)_2][PF_6]$ was unsuccessful but the addition of 1 equivalent of *trans*-$[Mn(CN)(CO)(dppm)_2]^+$ to $[Fe(PPh_3)_2(NO)_2]^+$ in CH_2Cl_2 gave a blue-green solution, the IR spectrum of which showed bands at 2090m [ν(CN)], 1958s [ν(CO)] and 1812ms and 1754s cm^{-1} [ν(NO)]. This spectrum, and in particular the shifts in ν(CN) (+48 cm^{-1}) and ν(NO) (+10–15 cm^{-1}) compared with $\mathbf{7}^+$ is consistent with the formation of $\mathbf{7}^{2+}$; the higher positive charge on the Mn^{II} centre inhibits π back bonding to the π* CN and π* NO orbitals. The addition of *n*-hexane to the reaction mixture gave a blue-green solid which proved insufficiently stable for further characterisation. However, a rotating platinum electrode voltammogram of this species in CH_2Cl_2, directly generated in the electrochemical cell by the chemical reaction between *trans*-$[Mn(CN)(CO)(dppm)_2]^+$ and $[Fe(PPh_3)_2(NO)_2]^+$ (1:1), showed two reversible reduction waves. The potentials of these waves were identical to those for the oxidation and reduction (see below) of $\mathbf{7}^+$, providing further evidence for the existence of $\mathbf{7}^{2+}$. Solutions apparently containing $\mathbf{7}^{2+}$ were ESR inactive. In the absence of solid-state magnetic susceptibility data, however, the possibility of diamagnetic coupling of the two 17-electron metal centres (formally Mn^{II} and Fe^{-I}) across the cyanide bridge could not be confirmed.

The cyclic voltammograms of $\mathbf{5}^+$–$\mathbf{7}^+$ also showed reduction waves, at −0.18, −0.13 and −0.28 V respectively, which are reversible at scan rates of 100 mV s^{-1} and greater. Substitution of I^- in **1–3** by the better π-acceptor ligand, PPh_3, is sufficient to stabilise the Fe^{-II} species $\mathbf{5}^+$–$\mathbf{7}^+$, at least on the cyclic voltammetric time-scale. In addition, the electron-transfer process occurs at a much more positive potential than those for **1–3** (by *ca.* 0.6 V) rendering the reduced products **5–7** more chemically accessible.

The reduction wave for $\mathbf{7}^+$ is equal in height to that of the oxidation wave discussed above, implying that reduction also involves a one-electron transfer. This observation, combined with the reversibility and potential of the process suggested that neutral **7** might be readily isolable from $\mathbf{7}^+$. On adding 1 equivalent of $[Co(\eta\text{-}C_5H_5)_2]$ to $\mathbf{7}^+$ in CH_2Cl_2 the solution rapidly changed from blue to brown. The product decomposed very rapidly and could not be isolated but the initial IR spectrum of the reaction mixture showed bands at 2097 [ν(CN)], 1918 [ν(CO)] and 1688 and 1637 [ν(NO)] cm^{-1}, consistent with the formation of **7**. The large shift of ν(NO) to lower energy (*ca.* 110 cm^{-1}) is similar to that observed [16] when $[Fe(PPh_3)_2(NO)_2]^+$ is reduced to $[Fe(PPh_3)_2(NO)_2]$ [Δν(NO) = *ca.* 100 cm^{-1}] implying reduction of the iron to Fe^{-II}. The shift to higher energy in the cyanide stretching frequency [Δν(CN) = 43 cm^{-1}] is also consistent with reduction at the N bound end of the Mn–CN–Fe unit; the less positive charge of the iron atom leads to less π back donation from Mn to the π* CN orbitals.

Heterotrinuclear complexes $[FeL_2(NO)_2]^+$ (L = cyanomanganese ligand)

In order to investigate the interaction of two redox-active Mn^I sites co-ordinated to a third metal centre, we have synthesised heterotrinuclear derivatives of square planar Rh^I [10] and linear Cu^I, Ag^I and Au^I.[11] We now describe the co-ordination of two cyanomanganese ligands to a paramagnetic, tetrahedral dinitrosyliron(−I) centre.

The complexes $[Fe\{(\mu\text{-}NC)MnL_x\}_2(NO)_2][PF_6]$ {L_x = *trans*-$(CO)_2[P(OEt)_3](dppm)$ $\mathbf{9}^+$ and *cis*-$(CO)_2(PEt_3)(dppe)$ $\mathbf{10}^+$} were synthesised by two methods. {The complex containing *trans*-$[Mn(CN)(CO)(dppm)_2]$ as the ligand could not be prepared.} First, the iodide complexes **1** and **2** react with 1 equivalent of the appropriate mononuclear complex {*trans*-$[Mn(CN)(CO)_2\{P(OEt)_3\}(dppm)]$ and *cis*-$[Mn(CN)(CO)_2(PEt_3)(dppe)]$ respectively} in the presence of $TlPF_6$ to give dark brown solutions from which black oils were isolated on addition of *n*-hexane. Treatment of CH_2Cl_2 solutions of the oils with *n*-hexane and trituration of the resulting precipitates with diethyl ether then gave $\mathbf{9}^+$ and $\mathbf{10}^+$ as dark brown solids which were characterised by elemental analysis and IR spectroscopy (Table 1). Secondly $\mathbf{9}^+$ and $\mathbf{10}^+$ can be prepared by adding 2 equivalents of *trans*-$[Mn(CN)(CO)_2\{P(OEt)_3\}(dppm)]$ or *cis*-$[Mn(CN)(CO)_2(PEt_3)(dppe)]$ to $[Fe(PPh_3)_2(NO)_2][PF_6]$ in CH_2Cl_2. Surprisingly, in this reaction both PPh_3 ligands are displaced from the dinitrosyl cation by the cyanomanganese ligands; the σ donor $OPPh_3$ displaces only one.[16]

The IR spectra of $\mathbf{9}^+$ and $\mathbf{10}^+$ (Table 1) show carbonyl bands very similar in energy to those of the iodo and PPh_3 analogues described above. The cyanide bands and the average values of

the two nitrosyl bands for both 9^+ and 10^+ are intermediate in energy between those of the iodo and PPh_3 analogues, again showing the cyanomanganese ligands to be better net electron donors than PPh_3.

The cyclic voltammogram of 9^+ shows an oxidation peak at 0.99 V with an associated reduction peak at 0.79 V. Although this wave appeared to be reversible (i_{red}/i_{ox} = 1.03 at 200 mV s^{-1}), the peak-to peak separation of 200 mV and the broadening of the reduction peak probably indicate some decomposition after oxidation. No assessment of the number of electrons involved in the oxidation process was possible but the wave height is approximately twice that of the reduction wave (see below), as expected if two Mn^I sites are oxidised and one Fe^{-I} site is reduced. A differential-pulse voltammogram of 9^+ showed only one oxidation wave, indicating no significant interaction between the two redox sites in 9^+. The square-planar complex $[Rh(CO)_2\{(\mu\text{-}NC)MnL_x\}_2]$ $\{L_x$ = *trans*-$(CO)_2[P(OEt)_3](dppm)\}$ showed[5] two waves separated by *ca.* 80 mV, indicating a weak interaction between the two Mn-based redox centres. The cyclic voltammogram of 10^+ showed an irreversible oxidation peak at 1.13 V associated with two small, overlapping reduction peaks at *ca.* 0.76 V and 0.71 V. The single oxidation peak again suggests that there is no communication between the redox sites; two product waves indicate at least partial decomposition after oxidation.

The cyclic voltammograms of 9^+ and 10^+ also show irreversible reduction peaks, at −0.76 and −0.68 V respectively. A comparison with the reduction potentials for 5^+ (−0.18), 6^+ (−0.13) and $[Fe(PPh_3)_2(NO)_2]^+$ (0.37 V) shows that replacement of each PPh_3 ligand by a cyanomanganese ligand causes the dinitrosyliron fragment to become substantially more difficult to reduce. Moreover, the reduction process becomes less reversible. These observations are in full accord with (*i*) the IR spectroscopic data [ν(NO), Table 1], which show the greater net electron-donor ability of the cyanomanganese ligands compared with PPh_3, and (*ii*) the suggestion[15] that better π-accepting ligands are required to stabilise the lower oxidation state Fe^{-II} in $[FeL_2(NO)_2]$ complexes.

One final experiment is of note. The addition of 1 equivalent of $[Fe(PPh_3)_2(NO)_2]^+$ to 9^+ or 10^+ in CH_2Cl_2 results in the rapid and quantitative formation of blue solutions of 6^+ and 7^+ respectively (confirmed by IR spectroscopy and cyclic voltammetry). The mechanism of this reaction is unclear. Although $[Fe(PPh_3)_2(NO)_2]^+$ is labile to substitution by the manganese ligands, the heterotrinuclear complexes do not appear to react with PPh_3.

ESR Spectroscopic studies

Room temperature ESR spectra of complexes **1**–**4** in toluene or CH_2Cl_2–$C_2H_4Cl_2$ (1:1) consist of six lines due to hyperfine coupling to ^{127}I ($I = \frac{5}{2}$); parameters are given in Table 4. The lines are broad (*ca.* 13 G) compared with those of $[Fe(PPh_3)_2(NO)_2]^+$ and $[Fe(OPPh_3)(PPh_3)(NO)_2]^+$ (*ca.* 1.0 G).[16] Frozen-solution spectra of these complexes are poorly resolved and could not be interpreted with confidence, but it is clear that the *g* matrix anisotropy is substantial, accounting, at least in part, for the broad lines of the isotropic spectra. The isotropic ^{127}I couplings, $\langle a^I \rangle$ = 18.8–19.5 G, are quite similar to the 20.2 G coupling reported[18] for $[FeI_2(NO)_2]^-$, consistent with the similar tetrahedral arrangement of ligands about the Fe atom, as noted above. Indeed, the frozen-solution spectra of **1**–**4** are qualitatively similar to that of the diiodide anion. Although Bryar and Eaton[18] report parameters for the frozen-solution spectrum of $[FeI_2(NO)_2]^-$, a simulation based on those parameters is in very poor agreement with the experimental spectrum and we regard the parameters as unreliable.

The ESR spectra of the complexes 6^+–8^+ are shown in Fig. 2. The lines are narrower (*ca.* 2.2 G for 7^+ and *ca.* 1.7 G for 6^+ and 8^+) than those for **1**–**4**. Each spectrum consists of a doublet of multiplets; 12 multiplet lines for 6^+ and 7^+, 10 for 8^+. The large doublet splitting is due to hyperfine coupling to ^{31}P ($I = \frac{1}{2}$) of the PPh_3 ligand on the iron fragment. The smaller splittings are due to hyperfine coupling to the two nitrosyl ^{14}N nuclei (I = 1), to the ^{55}Mn nucleus ($I = \frac{5}{2}$) and, for 6^+ and 7^+, to the cyanide nitrogen. These spectra were analysed using a non-linear least-squares method[20] to fit the multiplet couplings and linewidths. Computer simulations based on the parameters of Table 4 are shown as the plotted symbols in Fig. 2. The quality of the analyses was somewhat reduced by the presence of a small amount of $[Fe(PPh_3)_2(NO)_2]^+$ in the solutions (weak lines to the left of centre in the spectra shown in Fig. 2). The spectrum of 5^+ is qualitatively similar to those of 6^+–8^+ but was less well resolved and not subjected to detailed analysis. The frozen-solution spectrum of 6^+ exhibits three features, each split into a doublet by ^{31}P hyperfine coupling, but only the g_{min} features are well resolved; the spectrum was analysed by comparison with computer simulations to give the parameters listed in Table 4.

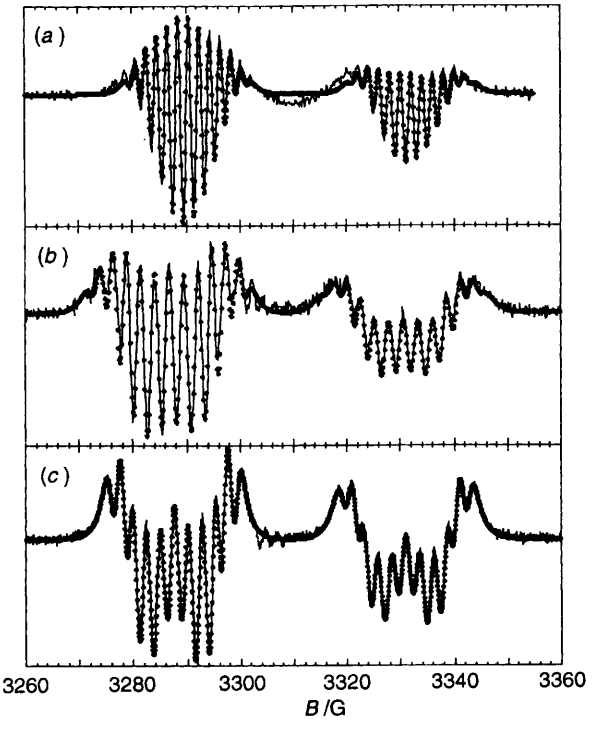

Fig. 2 Second-derivative ESR spectra of (*a*) 6^+, (*b*) 7^+ and (*c*) 8^+ in CH_2Cl_2 at 300 K. Plotted symbols represent computer simulations based on the parameters contained in Table 4(*b*)

The ^{31}P couplings for 5^+–8^+, $\langle a^P \rangle$ = 42–44 G, are much closer to the 45.7 G coupling found[1–6] for $[Fe(OPPh_3)(PPh_3)(NO)_2]^+$ than to the 13.8 G coupling for $[Fe(PPh_3)_2(NO)_2]^+$. The anisotropic parameters for 6^+ are also very close to those for $[Fe(OPPh_3)(PPh_3)(NO)_2]^+$ [g = 2.013, 2.034, 2.049; A^P = 53.9, 42.9, 29.7 ($\times 10^{-4}$ cm^{-1})]. This suggests that, unlike **1**–**4**, the structures of 5^+–8^+ are significantly distorted from tetrahedral.

The linewidth parameters, β and γ, found in fitting the isotropic spectra of 6^+–8^+, should be proportional to the rotational correlation time. Using the experimental g and A^P matrix components for 6^+ and equations given elsewhere,[20] the value of β_P leads to a rotational correlation time, τ_r = 8×10^{-11} s. Since $\tau_r = V_h\eta/T$, where V_h is the effective hydrodynamic volume of the complex and η is the viscosity, we expect τ_r to increase with steric bulk. We find that β_P increases in the order $6^+ < 8^+ < 7^+$, consistent with the expected volumes and suggesting that the g and A^P anisotropies of 7^+ and 8^+ are comparable with those for 6^+.

Table 4 The ESR spectroscopic data for $[FeL'_n\{(\mu\text{-NC})MnL_x\}_{2-n}(NO)_2]^z$

(*a*) Isotropic parameters for $[FeI\{(\mu\text{-NC})MnL_x\}(NO)_2]$

Complex	L_x	$\langle g \rangle$	$\langle a^I \rangle$/G	T/K
1[a]	*trans*-$(CO)_2[P(OEt)_3]$(dppm)	2.0553	19.5	300
2[a]	*cis*-$(CO)_2(PEt_3)$(dppe)	2.0601	18.8	310
3[b]	*trans*-(CO)$(dppm)_2$	2.0551	19.5	280
4[b]	*trans*-$(CO)_2[P(OPh)_3]$(dppm)	2.0562	19.2	290

(*b*) Isotropic parameters for $[Fe(PPh_3)\{(\mu\text{-NC})MnL_x\}(NO)_2]^+$ [c]

Complex	L_x	$\langle g \rangle$	Hyperfine couplings/G		Linewidth parameters/G		T/K
$\mathbf{5}^+$	*trans*-$(CO)_2[P(OEt)_3]$(dppm)	2.0331	$\langle a^P \rangle$	44.0(0)	—		280
$\mathbf{6}^+$	*cis*-$(CO)_2(PEt_3)$(dppe)	2.0336	$\langle a^P \rangle$	41.63(1)	α	1.71(1)	Room temperature
			$\langle a^{Mn} \rangle$	2.01(1)	β_P	−0.27(1)	
			$\langle a^{N(O)} \rangle$	1.721(6)	β_{Mn}	0.007(8)	
			$\langle a^{N(C)} \rangle$	2.14(2)	$\beta_{N(O)}$	0.103(6)	
$\mathbf{7}^+$	*trans*-(CO)$(dppm)_2$	2.0324	$\langle a^P \rangle$	43.84(4)	α	2.16(2)	290
			$\langle a^{Mn} \rangle$	2.833(4)	β_P	−0.48(3)	
			$\langle a^{N(O)} \rangle$	2.32(4)	β_{Mn}	0.000(4)	
			$\langle a^{N(C)} \rangle$	2.15(2)	γ_{Mn}	0.022(2)	
					$\beta_{N(O)}$	0.05(1)	
$\mathbf{8}^+$	*trans*-$(CO)_2[P(OPh)_3]$(dppm)	2.0340	$\langle a^P \rangle$	43.34(2)	α	1.63(1)	300
			$\langle a^{Mn} \rangle$	2.750(2)	β_P	−0.30(1)	
			$\langle a^{N(O)} \rangle$	2.020(2)	β_{Mn}	0.014(3)	
			$\langle a^{N(C)} \rangle$	0.55(5)	γ_{Mn}	0.029(1)	
					$\beta_{N(O)}$	0.014(2)	

(*c*) Isotropic parameters for $[Fe\{(\mu\text{-NC})MnL_x\}_2(NO)_2]^+$ [c,d]

Complex	L_x	$\langle g \rangle$
$\mathbf{9}^+$	*trans*-$(CO)_2\{P(OEt)_3\}$(dppm)	2.0330
$\mathbf{10}^+$	*cis*-$(CO)_2(PEt_3)$(dppe)	2.0338

(*d*) Anisotropic parameters[e]

Complex	g_1	g_2	g_3	A_1[f]	A_2[f]	A_3[f]
$\mathbf{6}^+$	2.012	2.036	2.055	49.6(2)	42(1)	33(2)
$\mathbf{9}^+$	2.014	2.027	2.054	—	—	—

[a] In toluene solution. [b] In CH_2Cl_2–$C_2H_4Cl_2$ (1:1) solution. [c] In CH_2Cl_2. [d] At 300 K. [e] In frozen CH_2Cl_2–$C_2H_4Cl_2$ (1:1) at 77 K. [f] Hyperfine couplings in units of 10^{-4} cm^{-1}.

In considering the coupling constants and linewidth parameters due to N(O) and Mn, we confine our attention to $\mathbf{8}^+$, for which the fit was generally the most reliable. Here we find $\langle a^{N(O)} \rangle = 2.020 \pm 0.002$ G and $\beta_{N(O)}/\beta_P = -0.046 \pm 0.007$, virtually identical to the corresponding coupling (1.998 ± 0.002 G) and ratio (−0.048 ± 0.002) for $[Fe(OPPh_3)(PPh_3)(NO)_2]^+$. Since the P hyperfine matrices are very similar for the two species, these results suggest similar N(O) 2p spin densities as well. The isotropic ^{55}Mn coupling and linewidth parameters suggest significant spin density on Mn. There are several ways of estimating the Mn contribution to the singly occupied molecular orbital (SOMO). For species such as *trans*-$[Mn(CO)(CN)(dppm)_2]^+$, $\langle a^{Mn} \rangle \approx 60$ G where the Mn 3d contribution to the SOMO is $\rho_{3d} \approx 0.7$;[6] assuming that $\langle a^{Mn} \rangle$ is proportional to ρ_{3d}, $\langle a^{Mn} \rangle = 2.75$ G suggests $\rho_{3d} \approx 0.03$. Assuming that the g anisotropy is the same as for $\mathbf{6}^+$, the parameter $\beta_{Mn} = 0.014$ G leads to $0.005 < \rho_{3d} < 0.02$, depending on the relative orientations of the $g_{\|}$ and $A_{\|}$ principal axes. Assuming that $\tau_r \approx 8 \times 10^{-11}$ s, the parameter $\gamma_{Mn} = 0.029$ G leads to $\rho_{3d} \approx 0.1$. The first estimate is probably the most reliable, but in any case, the appearance of a ^{55}Mn coupling clearly indicates significant delocalisation of the SOMO onto the Mn atom.

The appearance of coupling to the cyanide nitrogen is expected since that atom is bound to iron, the position of greatest spin density; such a coupling is not resolved in spectra of the mononuclear Mn^{II} species.[6] The ^{14}N coupling in the spectra of $\mathbf{6}^+$ and $\mathbf{7}^+$ is significantly greater than the corresponding coupling in the spectrum of $\mathbf{8}^+$, thus the 12-line multiplets for $\mathbf{6}^+$ and $\mathbf{7}^+$ and the 10-line multiplets for $\mathbf{8}^+$. (Although the least-squares fitting procedure regarded this nitrogen coupling as statistically significant in the spectrum of $\mathbf{8}^+$, its contribution was to the line shape rather than to separate features.) It is not obvious, however, why this coupling should be so different in these spectra.

The ESR spectra of $\mathbf{9}^+$ and $\mathbf{10}^+$ in CH_2Cl_2 at 300 K each consist of a single broad line (*ca.* 13 G wide), almost certainly masking unresolved hyperfine structure. The frozen-solution spectrum of $\mathbf{9}^+$ consists of three broad features with no hyperfine coupling. Parameters are given in Table 4. The g components for $\mathbf{9}^+$ are similar to those of the mononuclear complexes, $[Fe(PPh_3)_2(NO)_2]^+$, $[Fe(PPh_3)(OPPh_3)(NO)_2]^+$ and $[Fe(OPPh_3)_2(NO)_2]^+$,[16] but, since no hyperfine structure was resolved, the spectra give no structural information, and we can conclude only that $\mathbf{9}^+$ is also an Fe^{-1} complex.

Conclusion

Cyanide bridged complexes $[FeI\{(\mu\text{-NC})MnL_x\}(NO)_2]$, $[Fe(PPh_3)\{(\mu\text{-NC})MnL_x\}(NO)_2][PF_6]$ and $[Fe\{(\mu\text{-NC})MnL_x\}_2(NO)_2][PF_6]$, containing redox-active manganese ligands bound to the paramagnetic dinitrosyliron fragment, have been synthesised. Single crystal X-ray studies show the structure of $[FeI\{(\mu\text{-NC})Mn(CO)(dppm)_2\}(NO)_2]$ to be similar to that of $[FeI_2(NO)_2]^-$, in agreement with the results of ESR spectroscopy; the spectra of $[Fe(PPh_3)\{(\mu\text{-NC})MnL_x\}(NO)_2]^+$, however, suggest a distortion from tetrahedral geometry.

Cyclic voltammetric studies of $[Fe\{(\mu\text{-NC})MnL_x\}_2(NO)_2]^+$ suggest little interaction between the two redox-active Mn centres across the CN–$Fe(NO)_2$–NC bridge; the observation of ^{55}Mn and ^{14}N coupling in the ESR spectra of $[Fe(PPh_3)\{(\mu\text{-NC})MnL_x\}(NO)_2]^+$, however, suggests small but significant delocalisation of the SOMO through the NC bridge to Mn.

Experimental

The preparation, purification and reactions of the complexes described were carried out under an atmosphere of dry nitrogen or argon using dried, distilled and deoxygenated solvents; reactions were monitored by IR spectroscopy where necessary. Unless stated otherwise (*i*) complexes were purified by dissolution in CH_2Cl_2, filtration through Celite, addition of *n*-hexane and reduction of the volume of the mixture *in vacuo* to induce precipitation, and (*ii*) are stable under nitrogen and dissolve in polar solvents such as CH_2Cl_2 and tetrahydrofuran (thf) to give moderately air-sensitive solutions. The compounds $[\{Fe(\mu\text{-}I)(NO)_2\}_2]$,[21] $[Fe(PPh_3)_2(NO)_2]^+$,[16] $[Fe(\eta\text{-}C_5H_5)_2][PF_6]$,[22] $[Co(\eta\text{-}C_5H_5)_2]$,[23] *cis*- and *trans*-$[Mn(CN)(CO)_2\{P(OR)_3\}(dppm)]$ (R = Et[7] or Ph[24]), *cis*-$[Mn(CN)(CO)_2(PEt_3)(dppe)]$[7] and *trans*-$[Mn(CN)(CO)_2(PR_3)(L\text{–}L)][PF_6]$ (R = OEt or OPh, L–L = dppm; R = Et, L–L = dppe),[8] *trans*-$[Mn(CN)(CO)(dppm)_2]$ and *trans*-$[Mn(CN)(CO)(dppm)_2][PF_6]\cdot CH_2Cl_2$[9] were prepared by published methods. The salt $TlPF_6$ was purchased from Strem Chemicals. Infrared spectra were recorded on a Nicolet 5ZDX FT spectrometer. X-Band ESR spectra were recorded on a Bruker ESP-300E spectrometer equipped with a Bruker variable-temperature accessory and a Hewlett Packard 5350B microwave frequency counter. The field calibration was checked by measuring the resonance of the diphenylpicrylhydrazyl (dpph) radical before each series of spectra. Electrochemical studies were carried out using an EG and G model 273 potentiostat in conjunction with a three-electrode cell. For cyclic voltammetry the auxiliary electrode was a platinum wire and the working electrode a platinum disc. The reference was an aqueous saturated calomel electrode separated from the test solution by a fine-porosity frit and an agar bridge saturated with KCl. Voltammetry used a platinum disc electrode rotated at 600 revolutions min^{-1}. Differential-pulse voltammetry was carried out using the EG and G model 270 Electrochemical Analysis software. Solutions were 0.1×10^{-3} mol dm^{-3} in the test compound and 0.1 mol dm^{-3} in $[NBu^n_4][PF_6]$ as the supporting electrolyte. Under these conditions, $E^{\circ\prime}$ for the couples $[Fe(\eta\text{-}C_5H_5)_2]^+$–$[Fe(\eta\text{-}C_5H_5)_2]$ and $[Fe\{\eta\text{-}C_5H_4(COMe)\}_2]^+$–$[Fe\{\eta\text{-}C_5H_4(COMe)\}_2]$, added to the test solutions as internal calibrants, are 0.47 and 0.97 V respectively. Microanalyses were carried out by the staff of the Microanalytical Service of the School of Chemistry, University of Bristol.

Syntheses

$[FeI\{(\mu\text{-}NC)MnL_x\}(NO)_2]$ 2 [L_x = *cis*-$(CO)_2(PEt_3)(dppe)$]. To a stirred solution of $[\{Fe(\mu\text{-}I)(NO)_2\}_2]$ (0.11 g, 0.23 mmol) in CH_2Cl_2 (40 cm^3) was added *cis*-$[Mn(CN)(CO)_2(PEt_3)(dppe)]$ (0.30 g, 0.45 mmol). The brown solution was filtered through Celite, *n*-hexane added and the volume of the mixture reduced *in vacuo* to induce precipitation. The product was purified from CH_2Cl_2–*n*-hexane to give brown microcrystals, yield 284 mg (70%).

The complexes $[FeI\{(\mu\text{-}NC)MnL_x\}(NO)_2]$ {L_x = *trans*-$(CO)_2[P(OEt)_3](dppm)$ **1** and *trans*-$(CO)(dppm)_2$ **3**} were prepared similarly; the former was purified from diethyl ether–*n*-hexane.

$[Fe(PPh_3)\{(\mu\text{-}NC)MnL_x\}(NO)_2][PF_6]$ 6^+ [L_x = *cis*-$(CO)_2(PEt_3)(dppe)$]. To a stirred solution of $[Fe(PPh_3)_2(NO)_2][PF_6]$ (141 mg, 0.18 mmol) in CH_2Cl_2 (35 cm^3) was added *cis*-$[Mn(CN)(CO)_2(PEt_3)(dppe)]$ (117 mg, 0.18 mmol). The blue solution was filtered through Celite, *n*-hexane added and the volume of the mixture reduced *in vacuo* to induce precipitation. The product was purified from CH_2Cl_2–*n*-hexane, giving a blue oil; trituration with diethyl ether gave a blue solid, yield 127 mg (68%).

The complex $[Fe(PPh_3)\{(\mu\text{-}NC)MnL_x\}(NO)_2][PF_6]$ 5^+ {L_x = *trans*-$(CO)_2[P(OEt)_3](dppm)$} was prepared similarly.

$[Fe(PPh_3)\{(\mu\text{-}NC)MnL_x\}(NO)_2][PF_6]$ 7^+ [L_x = *trans*-$(CO)(dppm)_2$]. To a stirred solution of $[Fe(PPh_3)_2(NO)_2][PF_6]$ (187 mg, 0.24 mmol) in CH_2Cl_2 (35 cm^3) was added *trans*-$[Mn(CN)(CO)(dppm)_2]$ (198 mg, 0.24 mmol). The blue-green solution was filtered through Celite, *n*-hexane added and the volume of the mixture reduced *in vacuo* to induce precipitation. The product was purified by fractional crystallisation from CH_2Cl_2–*n*-hexane, the first fraction being discarded, to give blue-green microcrystals, yield 175 mg (53%).

$[Fe\{(\mu\text{-}NC)MnL_x\}_2(NO)_2][PF_6]$ 9^+ {L_x = *trans*-$(CO)_2[P(OEt)_3](dppm)$}. To a stirred solution of $[Fe(PPh_3)_2(NO)_2][PF_6]$ (150 mg, 0.19 mmol) in CH_2Cl_2 (50 cm^3) was added *trans*-$[Mn(CN)(CO)_2\{P(OEt)_3\}(dppm)]$ (263 mg, 0.38 mmol). The dark brown solution was filtered through Celite, *n*-hexane added and the volume of the mixture reduced *in vacuo* to induce precipitation. The product was purified from CH_2Cl_2–*n*-hexane, giving a black oil; trituration with diethyl ether gave a dark brown solid, yield 284 mg (73%).

$[Fe\{(\mu\text{-}NC)MnL_x\}_2(NO)_2][PF_6]$ 10^+ [L_x = *cis*-$(CO)_2(PEt_3)(dppe)$]. A mixture of $[FeI\{(\mu\text{-}NC)MnL_x\}(NO)_2]$ [L_x = *cis*-$(CO)_2(PEt_3)(dppe)$] (0.50 g, 0.56 mmol), *cis*-$[Mn(CN)(CO)_2(PEt_3)(dppe)]$ (365 mg, 0.558 mmol) and $TlPF_6$ (0.214 g, 0.56 mmol) in CH_2Cl_2 (75 cm^3) was stirred until the reaction was adjudged complete by IR spectroscopy (*ca.* 2.5 h). The dark brown solution was filtered through Celite, *n*-hexane added and the volume of the mixture reduced *in vacuo* to induce precipitation. The product was purified from CH_2Cl_2–*n*-hexane, giving a black oil; trituration with diethyl ether gave a dark brown solid, yield 433 mg (50%).

Crystal structure analysis for $3\cdot CH_2Cl_2$

Crystal data. $C_{53}H_{46}Cl_2F_4FeIMnN_3O_3P$, M = 1205.4, triclinic, space group $P\bar{1}$ (no. 2), a = 14.160(5), b = 14.794(6), c = 14.865(8) Å, α = 88.83(4), β = 75.45(4), γ = 64.66(3)°, U = 2709(2) $Å^3$, Z = 2, D_c = 1.48 g cm^{-3}, λ = 0.710 73 Å, μ = 1.33 mm^{-1}, $F(000)$ = 1214, T = 293 K.

Diffraction measurements were made with a Siemens four-circle R3m/V diffractometer using graphite-monochromated Mo-Kα X-radiation on a single crystal (approximate dimensions 0.50 × 0.30 × 0.25 mm) mounted in a thin-walled capillary under nitrogen. Cell dimensions were determined from the setting angle values of 36 centred reflections. A total of 8192 diffracted intensities (including checks) was measured in unique hemisphere of reciprocal space for $4.0 < 2\theta < 46.0°$ by Wyckoff ω scans. Three check reflections, remeasured after every 100 ordinary data, showed 31% decay over the period of data collection; a corresponding correction was applied. Of the 7593 non-check intensity data collected, 7074 unique observations remained after averaging of duplicate and equivalent measurements (R_{int} = 0.043) and deletion of systematic absences. Of these, 4028 with $I > 2\sigma(I)$ were retained for use in structure solution and refinement. An absorption correction was applied on the basis of 223 azimuthal scan data; maximum and minimum transmission coefficients were 0.800 and 0.477 respectively. Lorentz and polarisation corrections were applied. The structure was solved by heavy atom (Patterson and Fourier-difference) methods, and refined by full-matrix least squares against F. All atoms heavier than carbon, and C(1) and C(2), were assigned anisotropic displacement parameters while other carbon atoms were assigned isotropic displacement parameters. All non-hydrogen atoms were refined without positional constraints. Hydrogen atoms were constrained to idealised geometries (C–H 0.96 Å) and assigned a fixed isotropic displacement parameter. Refinement of the 363 least-squares variables converged smoothly to residual indices R = 0.071, R' = 0.071, S = 1.66 {$R = \Sigma|\Delta|/\Sigma|F_o|$; $R' = [\Sigma w\Delta^2/\Sigma wF_o^2]^{\frac{1}{2}}$; $S = [\Sigma w\Delta^2/(N_o -$

$N_v)]^{\frac{1}{2}}$; $\Delta = F_o - F_c\}$. Weights, w, were set equal to $[\sigma_c^2(F_o) + gF_o^2]^{-1}$ where $\sigma_c^2(F_o)$ = variance in F_o due to counting statistics and $g = 0.0005$ was chosen to minimise the variation in S as a function of F_o. Final difference electron density maps showed no features outside the range $+0.81$ to -0.89 e Å^{-3}; the largest remaining features are within 1.3 Å of the iodine atom. All calculations were made with programs of the SHELXTL PLUS package.[25] Complex neutral-atom scattering factors were taken from ref. 26.

Atomic coordinates, thermal parameters, and bond lengths and angles have been deposited at the Cambridge Crystallographic Data Centre (CCDC). See Instructions for Authors, *J. Chem. Soc., Dalton Trans.*, 1996, Issue 1. Any request to the CCDC for this material should quote the full literature citation and the reference number 186/7.

Acknowledgements

We thank the EPSRC for research studentships (to F. L. A., N. C. B. and G. M. R.) and for funds to purchase an ESR spectrometer.

References

1 W. P. Fehlhammer and M. Fritz, *Chem. Rev.*, 1993, **93**, 1243.
2 See, for example, M. P. Garcia, M. V. Jimenez, F. J. Lahoz and L. A. Oro, *J. Chem. Soc., Dalton Trans.*, 1995, 917; T. Mallah, C. Auberger, M. Verdaguer and P. Veillet, *J. Chem. Soc., Chem. Commun.*, 1995, 61; P. Braunstein, D. Cauzzi, D. Kelly, M. Lanfranchi and A. Tiripicchio, *Inorg. Chem.*, 1993, **32**, 3373; R. D. Pike and G. Carpenter, *Organometallics*, 1993, **12**, 1416; H. Yuge and T. Iwamoto, *J. Chem. Soc., Dalton Trans.*, 1993, 2841; R. Singh and S. K. Dikshit, *Polyhedron*, 1993, **12**, 1697.
3 D. H. Johnston, C. L. Stern and D. F. Shriver, *Inorg. Chem.*, 1993, **32**, 5170.
4 A. J. Deeming, G. P. Proud, H. M. Dawes and M. B. Hursthouse, *J. Chem. Soc., Dalton Trans.*, 1988, 2475; *Polyhedron*, 1988, **7**, 651.
5 N. Zhu and H. Vahrenkamp, *Angew. Chem., Int. Ed. Engl.*, 1994, **33**, 2090; *J. Organomet. Chem.*, 1994, **472**, C5; F. Scandola, R. Argazzi, C. A. Bignozzi, C. Chiorboli, M. T. Indelli and M. A. Rampi, *Coord. Chem. Rev.*, 1993, **125**, 283; T. Buranda, Y. Lei and J. F. Endicott, *J. Am. Chem. Soc.*, 1992, **114**, 6916; G. Barrado, G. A. Carriedo, C. Diaz-Valenzuela and V. Riera, *Inorg. Chem.*, 1991, **30**, 4416; J. B. Cooper, T. M. Vess, W. A. Kalsbeck and D. W. Wertz, *Inorg. Chem.*, 1991, **30**, 2286; B. Oswald, A. K. Powell, F. Rashwan, J. Heinze and H. Vahrenkamp, *Chem. Ber.*, 1990, **123**, 243; *Coord. Chem. Rev.*, 1991, **111**.
6 G. A. Carriedo, N. G. Connelly, E. Perez-Carreno, A. G. Orpen, A. L. Rieger, P. H. Rieger, V. Riera and G. M. Rosair, *J. Chem. Soc., Dalton Trans.*, 1993, 3103.
7 G. A. Carriedo, N. G. Connelly, M. C. Crespo, I. C. Quarmby, V. Riera and G. H. Worth, *J. Chem. Soc., Dalton Trans.*, 1991, 315.
8 G. A. Carriedo, N. G. Connelly, S. Alvarez, E. Perez-Carreno and S. Garcia-Granda, *Inorg. Chem.*, 1993, **32**, 272.
9 A. Christofides, N. G. Connelly, H. J. Lawson, A. C. Loyns, A. G. Orpen, M. O. Simmonds and G. H. Worth, *J. Chem. Soc., Dalton Trans.*, 1991, 1595.
10 F. L. Atkinson, A. Christofides, N. G. Connelly, H. J. Lawson, A. C. Loyns, A. G. Orpen, G. M. Rosair and G. H. Worth, *J. Chem. Soc., Dalton Trans.*, 1993, 1441.
11 D. Bellamy, N. C. Brown, G. B. Carpenter, N. G. Connelly, J. G. Crossley, A. G. Orpen, A. L. Rieger, P. H. Rieger, G. M. Rosair and G. H. Worth, unpublished work.
12 D. A. Dows, A. Haim and W. K. Wilmarth, *J. Inorg. Nucl. Chem.*, 1961, **21**, 33.
13 N. G. Connelly, K. A. Hassard, B. J. Dunne, A. G. Orpen, S. J. Raven, G. A. Carriedo and V. Riera, *J. Chem. Soc., Dalton Trans.*, 1988, 1623, and refs. therein.
14 See, for example, B. F. G. Johnson and J. A. McCleverty, *Prog. Inorg. Chem.*, 1966, **7**, 277.
15 C. A. Bignozzi, R. Argazzi, J. R. Schoonover, K. C. Gordon, R. B. Dyer and F. Scandola, *Inorg. Chem.*, 1992, **31**, 5260.
16 F. L. Atkinson, H. E. Blackwell, N. C. Brown, N. G. Connelly, J. G. Crossley, A. G. Orpen, A. L. Rieger and P. H. Rieger, unpublished work.
17 A. G. Orpen, L. Brammer, F. H. Allen, O. Kennard, D. G. Watson and R. Taylor, *J. Chem. Soc., Dalton Trans.*, 1989, S1.
18 T. R. Bryar and D. R. Eaton, *Can. J. Chem.*, 1992, **70**, 1917.
19 R. H. Summerville and R. Hoffmann, *J. Am. Chem. Soc.*, 1976, **98**, 7240.
20 L. V. Casagrande, T. Chen, P. H. Rieger, B. H. Robinson, J. Simpson and S. J. Visco, *Inorg. Chem.*, 1984, **23**, 2019.
21 B. Haymore and R. D. Feltham, *Inorg. Synth.*, 1973, **14**, 81.
22 J. C. Smart and B. L. Pinsky, *J. Am. Chem. Soc.*, 1980, **102**, 1009.
23 R. B. King, *Organomet. Synth.*, 1965, **1**, 70.
24 G. A. Carriedo, M. C. Crespo, V. Riera, M. G. Sanchez, M. L. Valin, D. Moreiras and X. Solans, *J. Organomet. Chem.*, 1986, **302**, 47.
25 G. M. Sheldrick, SHELXTL PLUS, version 4.2, Siemens Analytical Instruments Inc., Madison, WI, 1990.
26 *International Tables for X-Ray Crystallography*, Kynoch Press, Birmingham, 1974, vol. 4.

Received 21*st December* 1995; *Paper* 5/08307I